Preprints of the 21st IFAC World Congress (Virtual)
Berlin, Germany, July 12-17, 2020

Optimization-based motion planning for multi-steered articulated vehicles ⋆

Oskar Ljungqvist * **Kristoffer Bergman** * **Daniel Axehill** *

* *Division of Automatic Control, Linköping University, 581 83 Linköping, Sweden, (e-mail: {oskar.ljungqvist, kristoffer.bergman, daniel.axehill}@liu.se).*

Abstract: The task of maneuvering a multi-steered articulated vehicle in confined environments is difficult even for experienced drivers. In this work, we present an optimization-based trajectory planner targeting low-speed maneuvers in unstructured environments for multi-steered N-trailer vehicles, which are comprised of a car-like tractor and an arbitrary number of interconnected trailers with fixed or steerable wheels. The proposed trajectory planning framework is divided into two steps, where a lattice-based trajectory planner is used in a first step to compute a resolution optimal solution to a discretized version of the trajectory planning problem. The output from the lattice planner is then used in a second step to initialize an optimal control problem solver, which enables the framework to compute locally optimal trajectories that start at the vehicle's initial state and reaches the goal state exactly. The performance of the proposed optimization-based trajectory planner is evaluated in a set of practically relevant scenarios for a multi-steered 3-trailer vehicle with a car-like tractor where the last trailer is steerable.

Keywords: Trajectory planning, articulated vehicles, tractor-trailer vehicles

1. INTRODUCTION

In recent years, there has been a growing demand within the transportation sector to increase efficiency and reduce environmental impact related to transportation of both people and goods. This has lead to an increased interest for large capacity (multi-) articulated buses (Michalek, 2019) and long tractor-trailer vehicle combinations (Islam et al., 2015). In order to improve these long vehicles' ability to maneuver in confined environments, some trailers (or wagons) can be equipped with steerable wheels. In the literature, these vehicles are commonly referred to as multi-steered N-trailer (MSNT) vehicles (Orosco-Guerrero et al., 2002), which is a generalization of single-steered N-trailer (SSNT) vehicles. Compared to an SSNT vehicle, the additional steering capability enables an MSNT vehicle to be more flexible and agile, on the expense of increased difficulty in manually maneuvering the vehicle by a human driver. These difficulties partially arise due to the vehicle's increased degrees of freedom which are hard to successfully cope with for a human operator, and because of the specific kinematic and dynamic properties of an MSNT vehicle (see, e.g., Tilbury et al. (1995); Michalek (2019); Orosco-Guerrero et al. (2002); Islam et al. (2015)). To aid the driver, several advanced driver assistance system concepts have been proposed to automatically steer the extra steerable wheel(s) in order to increase low-speed maneuverability or to reduce the so-called off-tracking effect during tight cornering (Odhams et al., 2011; Van De Wouw et al., 2015; Michalek, 2019; Varga et al., 2018).

Although a large amount of different motion planning techniques has been proposed in the literature for SSNT vehicles (see, e.g., Sekhavat et al. (1998); Lamiraux et al. (1999); Evestedt et al. (2016); Li et al. (2019); Ljungqvist et al. (2019)), there only exists a limited amount of work that considers the trajectory planning problem for special classes of MSNT vehicles (see e.g. Bushnell et al. (1995); Tilbury et al. (1995); Vidal-Calleja et al. (2002); Beyersdorfer and Wagner (2013); Yuan (2017)). As a consequence, there is still a need to develop a trajectory planner that is able to solve the trajectory planning problem for a generic MSNT vehicle with a car-like tractor that: i) can handle various state and input constraints, ii) allows a mixture of on-axle/off-axle hitched and steerable/non-steerable trailers, and iii) computes locally optimal trajectories by combining forward and backward motion.

The contribution of this work is a trajectory planning framework for an MSNT vehicle with a car-like tractor targeting low-speed maneuvers in confined and unstructured environments. The framework extends some techniques presented in our previous work in Ljungqvist et al. (2019) and is inspired by Bergman et al. (2019, 2020); Bergman and Axehill (2018). Here, a lattice-based trajectory planner is developed and used in a first step to compute a resolution optimal solution to a discretized version of the trajectory planning problem. The lattice planner uses a finite library of precomputed optimized maneuvers restricted to move the MSNT vehicle within a specified state-space discretization. In a second step, the output from the lattice planner is used to initialize a homotopy-based optimization step enabling the framework to compute locally optimal trajectories that starts at the vehicle's initial state and reaches the desired goal state exactly. To the best of the authors knowledge, this paper presents the first trajectory planning framework for a generic MSNT vehicle with a car-like tractor.

The reminder of the paper is organized as follows. In Section 2, the kinematic vehicle model and the trajectory planning problem for the considered MSNT vehicle are presented, as well as an overview of the proposed trajec-

⋆ This work was supported by the Strategic vehicle research and innovation programme (FFI/VINNOVA) and the Wallenberg Autonomous Systems and Softward Programme (WASP).

tory planning framework. In Section 3 and Section 4, the lattice-based trajectory planner and the homotopy-based optimization step are presented, respectively. Simulation results for an MS3T vehicle with a car-like tractor are presented in Section 5 and the paper is concluded in Section 6 by summarizing the contributions and discussing directions for future work.

2. KINEMATIC VEHICLE MODEL AND PROBLEM FORMULATION

The MSNT vehicle with a car-like tractor considered in this work is illustrated in Fig. 1. The multi-body vehicle is composed of $N+1$ vehicle segments, including a car-like tractor and N number of trailers that are equipped with steerable or non-steerable wheels. Each vehicle segment is characterized by a segment length $L_i > 0$ and a signed hitching offset M_i. Since low-speed maneuvers are considered in this work, a kinematic vehicle model is used. The model is based on the work in Michalek (2019) and is derived based on various assumptions such as the wheels are rolling without slipping and that the vehicle is operating on a flat surface. Moreover, it is assumed that the front wheel of the tractor is steerable and its rear wheel is non-steerable. The vehicle configuration consists of $4+N+S$ variables (Michalek, 2019) where $S \in \{1,\dots,N\}$ denotes the number of steerable trailers:

– the steering angle of the tractor's front wheel
$$\beta_0 \in \mathcal{Q}_0 = [-\bar{\beta}_0, \bar{\beta}_0], \quad \bar{\beta}_0 \in (0, \pi/2), \tag{1}$$
– the global position (x_N, y_N) and orientation θ_N of the Nth trailer in a fixed coordinate frame
$$\boldsymbol{q}_N = [\theta_N \ x_N \ y_N]^\mathsf{T} \in \mathbb{S} \times \mathbb{R}^2, \tag{2}$$
where $\mathbb{S} = (-\pi, \pi]$,
– for $i = 1,\dots,N$, a number of N constrained joint angles
$$\beta_i = \theta_{i-1} - \theta_i \in \mathcal{B}_i = [-\bar{\beta}_i, \bar{\beta}_i], \quad \bar{\beta}_i \in (0, \pi), \tag{3}$$
– and $S \in \{1,\dots,N\}$ number of steering angles associated with steerable trailer wheels
$$\gamma_s \in \mathcal{Q}_s = [-\bar{\gamma}_s, \bar{\gamma}_s], \quad \bar{\gamma}_s \in (0, \pi/2), \tag{4}$$
where index $s \in \mathcal{I}_s \subseteq \{1,\dots,N\}$ specifies which trailers that have steerable wheels. The configuration vector for the MSNT with a car-like tractor will be defined as
$$\boldsymbol{q} = \begin{bmatrix}\beta_0 \ \beta_1 \ \dots \ \beta_N \ \boldsymbol{\gamma}_s^\mathsf{T} \ \boldsymbol{q}_N^\mathsf{T}\end{bmatrix}^\mathsf{T} \in \mathcal{Q}, \tag{5}$$
where $\boldsymbol{\gamma}_s$ represents a vector of trailer steering angles, and $\mathcal{Q} = \mathcal{Q}_0 \times \mathcal{B}_1 \times \dots \times \mathcal{B}_N \times \underbrace{\mathcal{Q}_s \times \dots \times \mathcal{Q}_s}_{S \text{ times}} \times \mathbb{S} \times \mathbb{R}^2$.

The leading car-like tractor is described by a kinematic single-track vehicle model and its orientation θ_0 evolves as
$$\dot{\theta}_0 = v_0 \kappa_0(\beta_0), \tag{6}$$
where $\kappa_0(\beta_0) = \frac{\tan\beta_0}{L_0}$ is the curvature of the tractor and v_0 is the longitudinal velocity of its rear axle. The recursive formula for the transformation of the angular $\dot{\theta}_i$ and longitudinal v_i velocities between any two neighboring vehicle segments are given by (Michalek, 2019; Orosco-Guerrero et al., 2002):
$$\begin{bmatrix}\dot{\theta}_i \\ v_i\end{bmatrix} = \underbrace{\begin{bmatrix} -\frac{M_i}{L_i}\frac{\cos(\beta_i - \gamma_i)}{\cos\gamma_i} & \frac{\sin(\beta_i - \gamma_i + \gamma_{i-1})}{L_i \cos\gamma_i} \\ M_i \frac{\sin\beta_i}{\cos\gamma_i} & \frac{\cos(\beta_i + \gamma_{i-1})}{\cos\gamma_i} \end{bmatrix}}_{\boldsymbol{J}_i(\beta_i, \gamma_i, \gamma_{i-1})} \begin{bmatrix}\dot{\theta}_{i-1} \\ v_{i-1}\end{bmatrix}, \tag{7}$$
where γ_i denotes the steering angle of the ith trailer. For the car-like tractor, we have that $\gamma_0 \equiv 0$ since its rear axle is non-steerable. Note that if the jth trailer is non-steerable, it suffices to take $\gamma_j = 0$ in (7).

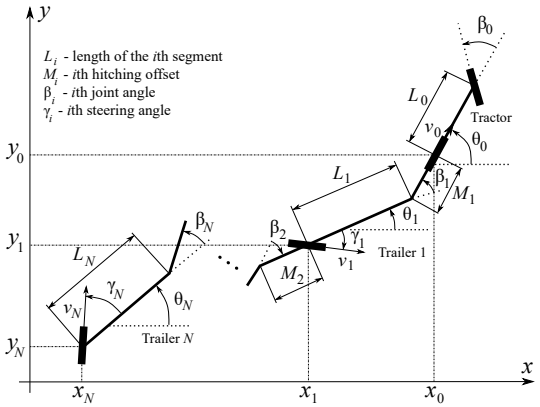

Fig. 1. A schematic description of the geometric lengths and the vehicle configuration for an MSNT vehicle with a car-like tractor in a global coordinate system (inspired and adapted from Michalek (2019)).

Each trailer's steering angle γ_s, $s \in \mathcal{I}_s$ and the tractors steering angle β_0 are modeled as double integrator systems
$$\begin{aligned} \dot{\gamma}_s &= \omega_s, \quad \dot{\omega}_s = u_{\omega_s}, \quad s \in \mathcal{I}_s, \\ \dot{\beta}_0 &= \omega_0, \quad \dot{\omega}_0 = u_{\omega_0}, \end{aligned} \tag{8}$$
where ω_0, ω_s, $s \in \mathcal{I}_s$ and u_{ω_0}, u_{ω_s}, $s \in \mathcal{I}_s$ denote steering angle rates and accelerations, respectively. This modeling is used to be able to penalize large rates and accelerations, and to enforce constraints in the form
$$\begin{aligned} &\omega_s \in \Omega_s = [-\bar{\omega}_s, \bar{\omega}_s], \quad u_{\omega_s} \in \mathcal{U}_s = [-\bar{\Omega}_s, \bar{\Omega}_s], \quad s \in \mathcal{I}_s, \\ &\omega_0 \in \Omega_0 = [-\bar{\omega}_0, \bar{\omega}_0], \quad u_{\omega_0} \in \mathcal{U}_0 = [-\bar{\Omega}_0, \bar{\Omega}_0], \end{aligned} \tag{9}$$
where the steering angle accelerations u_{ω_0} and u_{ω_s}, $s \in \mathcal{I}_s$ are treated as control signals. Similarly, the longitudinal velocity of the tractor v_0 is constrained as $v_0 \in \Omega_v = [-\bar{v}, \bar{v}]$ and its dynamics are modeled as a double integrator system
$$\dot{v}_0 = a_0, \quad \dot{a}_0 = u_v \tag{10}$$
in order to respect constraints on the longitudinal acceleration $a_0 \in \mathcal{A} = [-\bar{a}, \bar{a}]$ and jerk $u_v \in \mathcal{U}_v = [-\bar{u}_v, \bar{u}_v]$. During the planning phase, the longitudinal jerk u_v is treated as a control signal.

The position of the last trailer evolves according to standard unicycle kinematics
$$\begin{aligned} \dot{x}_N &= v_N \cos(\theta_N + \gamma_N), \\ \dot{y}_N &= v_N \cos(\theta_N + \gamma_N), \end{aligned} \tag{11}$$
where its angular rate $\dot{\theta}_N$ and longitudinal velocity v_N are given by
$$\begin{bmatrix}\dot{\theta}_N \\ v_N\end{bmatrix} = \prod_{i=0}^{N-1} \boldsymbol{J}_{N-i}(\beta_{N-i}, \gamma_{N-i}, \gamma_{N-i-1}) \begin{bmatrix}v_0\kappa_0 \\ v_0\end{bmatrix}, \tag{12}$$
which is derived by recursive usage of (7) N times together with (6). Combining (11) and (12), it is possible to compactly represent the model for the pose of the Nth trailer $\boldsymbol{q}_N = [\theta_N \ x_N \ y_N]^\mathsf{T}$ as $\dot{\boldsymbol{q}}_N = v_0 f_{\boldsymbol{q}_N}(\boldsymbol{q})$. In analogy, by introducing the vector $\boldsymbol{c}^\mathsf{T} = [1 \ 0]$ together with (6) and (7), the time derivative of (3) yields the joint-angle kinematics
$$\begin{aligned} \dot{\beta}_i = \dot{\theta}_{i-1} - \theta_i = \boldsymbol{c}^\mathsf{T} \prod_{j=N-i-1}^{N-1} \boldsymbol{J}_{N-j}(\beta_{N-j}, \gamma_{N-j}, \gamma_{N-j-1}) \begin{bmatrix}v_0\kappa_0 \\ v_0\end{bmatrix} \\ -\boldsymbol{c}^\mathsf{T} \prod_{j=N-i}^{N-1} \boldsymbol{J}_{N-j}(\beta_{N-j}, \gamma_{N-j}, \gamma_{N-j-1}) \begin{bmatrix}v_0\kappa_0 \\ v_0\end{bmatrix} \triangleq v_0 f_{\beta_i}(\boldsymbol{q}), \end{aligned} \tag{13}$$

for $i = 1, \ldots, N$. Introduce the augmented state vector $\boldsymbol{x}^\intercal = [\boldsymbol{q}^\intercal \ \omega_0 \ \boldsymbol{\omega}_s^\intercal \ v_0 \ a_0] \in \mathcal{X}$ and denote the control signal vector as $\boldsymbol{u}^\intercal = [u_{\omega_0} \ \boldsymbol{u}_{\boldsymbol{\omega}_s}^\intercal \ u_v] \in \mathcal{U}$, where $\boldsymbol{\omega}_s$ and $\boldsymbol{u}_{\boldsymbol{\omega}_s}$ represent vectors of trailer steering angle rates and accelerations, respectively, and

$$\begin{aligned} \mathcal{X} &= \mathcal{Q} \times \Omega_0 \times \underbrace{\Omega_s \times \ldots \times \Omega_s}_{S \text{ times}} \times \Omega_v \times \mathcal{A}, \\ \mathcal{U} &= \mathcal{U}_0 \times \underbrace{\mathcal{U}_s \times \ldots \times \mathcal{U}_s}_{S \text{ times}} \times \mathcal{U}_v, \end{aligned} \tag{14}$$

where $\dim(\mathcal{X}) = 7+N+2S \triangleq n$ and $\dim(\mathcal{U}) = 2 + S \triangleq m$. The constraints in (14) will be referred to the vehicle's physical constraints arising from, e.g., actuator, mechanical or sensing limitations. Finally, the kinematic model of the MSNT vehicle with a car-like tractor is given in (8), (10) and (11)–(13), which can be represented as

$$\dot{\boldsymbol{x}} = \boldsymbol{f}(\boldsymbol{x}, \boldsymbol{u}), \tag{15}$$

where $\boldsymbol{f} : \mathbb{R}^n \times \mathbb{R}^m \to \mathbb{R}^n$ is continuous and continuously differentiable with respect to $\boldsymbol{x} \in \mathcal{X}$ and $\boldsymbol{u} \in \mathcal{U}$.

2.1 Problem formulation

The MSNT vehicle with a car-like tractor is assumed to operate in a closed environment with only static obstacles $\mathcal{X}_{\text{obs}}$. The free-space where the vehicle is not in collision with any obstacle is defined as $\mathcal{X}_{\text{free}} = \mathcal{X} \setminus \mathcal{X}_{\text{obs}}$. Here, it is assumed that the obstacle-occupied region $\mathcal{X}_{\text{obs}}$ (hence also $\mathcal{X}_{\text{free}}$) can be described analytically, e.g., using different bounding regions (LaValle, 2006). Since the free-space $\mathcal{X}_{\text{free}}$ is defined as the complement set of $\mathcal{X}_{\text{obs}}$, it is in general a non-convex set.

The trajectory planning problem considered in this work is defined as follows: Compute a feasible and collision-free state and control signal trajectory $(\boldsymbol{x}(t), \boldsymbol{u}(t))$, $t \in [0, t_G]$ that moves the vehicle from its initial state $\boldsymbol{x}_I \in \mathcal{X}_{\text{free}}$ to a desired goal state $\boldsymbol{x}_G \in \mathcal{X}_{\text{free}}$, while minimizing the cost functional J. This problem can be posed as a continuous-time optimal control problem (OCP) in the following form

$$\begin{aligned} \underset{\boldsymbol{u}(\cdot),\, t_G}{\text{minimize}} \quad & J = t_G + \int_0^{t_G} l(\boldsymbol{x}(t), \boldsymbol{u}(t))\, dt \\ \text{subject to} \quad & \dot{\boldsymbol{x}}(t) = \boldsymbol{f}(\boldsymbol{x}(t), \boldsymbol{u}(t)), \\ & \boldsymbol{x}(0) = \boldsymbol{x}_I, \quad \boldsymbol{x}(t_G) = \boldsymbol{x}_G, \\ & \boldsymbol{x}(t) \in \mathcal{X}_{\text{free}}, \quad \boldsymbol{u}(t) \in \mathcal{U}, \end{aligned} \tag{16}$$

where the final time t_G and $\boldsymbol{u}$ are optimization variables, and $l : \mathbb{R}^n \times \mathbb{R}^m \to \mathbb{R}_+$ is called the Lagrange term or cost function. In this work, the cost function is defined as

$$l(\boldsymbol{x}, \boldsymbol{u}) = ||\boldsymbol{x}||_{\boldsymbol{Q}}^2 + ||\boldsymbol{u}||_{\boldsymbol{R}}^2, \tag{17}$$

where the weight matrices $\boldsymbol{Q} \succeq 0$ and $\boldsymbol{R} \succeq 0$. It is well-known that this OCP is in general hard to solve by directly invoking a state-of-the-art OCP solver (Andersson et al., 2018; Wächter and Biegler, 2006). This is mainly because the vehicle model is nonlinear and the free-space $\mathcal{X}_{\text{free}}$ is in many applications non-convex. Hence, a proper initialization strategy for any OCP solver is often a necessity in order for it to converge to a good locally optimal (or even feasible) solution (Bergman et al., 2020; Zhang et al., 2020).

2.2 Trajectory planning framework

To efficiently and reliably solve the trajectory planning problem (16) for an MSNT vehicle with a car-like tractor, we propose a framework that combines a lattice-based trajectory planner and an online optimization step. The framework is based on and extends the previous works in Ljungqvist et al. (2019); Bergman et al. (2019, 2020); Bergman and Axehill (2018). The extensions are made to account for the specific properties of an MSNT vehicle with a car-like tractor. The general idea is that a lattice-based trajectory planner is used in a first step to compute an optimal solution to a discrete version of the trajectory planning problem (16) using a discretized state-space and a library of precomputed trajectories. The lattice planner can be considered responsible for solving the combinatorial aspects of the trajectory planning problem, e.g., taking left or right around obstacles, and thus provides the latter optimization step with a proper initial guess. While keeping the combinatorial parts fixed, the objective of the optimization step is to further improve the initial guess computed by the lattice planner such that the resulting trajectory is a locally optimal solution to the original trajectory planning problem (16). However, since the lattice planner uses a discretized state space, in general its computed trajectory does not satisfies the initial and goal state constraints in (16). Therefore, the optimization step is also responsible for modifying the initial guess computed by the lattice planner such that the final optimized trajectory starts at the vehicle's initial state and reaches the goal state exactly. To handle this in a structured and numerically stable way, a homotopy-based optimization strategy is proposed that is inspired by the work in Bergman and Axehill (2018).

The main steps of the trajectory planning framework is summarized in Workflow 1, where the lattice planner (Step 0 and 1) and the optimization step (Step 2) are explained in detail in Section 3 and Section 4, respectively.

3. LATTICE-BASED TRAJECTORY PLANNER

The idea with lattice-based trajectory planning is to restrict the solutions of the trajectory planning problem (16) to a lattice graph $\mathcal{G} = \langle \mathcal{V}, \mathcal{E} \rangle$, which is a graph embedded in an Euclidean space that forms a regular and repeated pattern (Pivtoraiko et al., 2009). The lattice graph is constructed offline by discretizing the vehicle's state space $\mathcal{X}_d \subset \mathcal{X}$ and precompute a set of motion primitives $\mathcal{P}$. Each vertex $\boldsymbol{v}[k] \in \mathcal{V}$ is a vehicle state $\boldsymbol{x}[k] \in \mathcal{X}_d$ and each edge $\boldsymbol{e}_i \in \mathcal{E}$ represents of a motion primitive $\boldsymbol{m}_i \in \mathcal{P}$. A motion primitive is a feasible trajectory $(\boldsymbol{x}^i(t), \boldsymbol{u}^i(t))$, $t \in [0, t_f^i]$ that moves the vehicle from an initial state $\boldsymbol{x}[k] \in \mathcal{X}_d$ to a final state $\boldsymbol{x}[k+1] \in \mathcal{X}_d$ while satisfying $\boldsymbol{x}^i(\cdot) \in \mathcal{X}$ and $\boldsymbol{u}^i(\cdot) \in \mathcal{U}$. A motion primitive is in this way designed to connect two vertices in the graph and the kinematic constraints (15) and the physical constraints (14) are satisfied offline. The cardinality of the motion primitive set is $|\mathcal{P}| = M$ and the motion primitives that can be used from $\boldsymbol{x}[k]$ is denoted $\mathcal{P}(\boldsymbol{x}[k]) \subseteq \mathcal{P}$. Moreover, since the MSNT vehicle is position invariant, the motion primitive set $\mathcal{P}$ can be computed from the position of the Nth trailer at the origin. Each motion primitive $\boldsymbol{m}_i$ can then be translated and reused for all other positions on the grid.

Let $\boldsymbol{x}[k+1] = f_p(\boldsymbol{x}[k], \boldsymbol{m}_i)$ denote the successor state when motion primitive $\boldsymbol{m}_i \in \mathcal{P}$ is applied from $\boldsymbol{x}[k]$ and denote $J_p(\boldsymbol{m}_i)$ as the stage-cost associated to this transition, which is given by

$$J_p(\boldsymbol{m}_i) = t_f^i + \int_0^{t_f^i} l(\boldsymbol{x}^i(t), \boldsymbol{u}^i(t)), \tag{18}$$

Workflow 1 The proposed trajectory planning framework for a MSNT vehicle with a car-like tractor

Step 0 (offline) – State lattice construction:
a) ***State-space discretization:*** Specify the resolution of the discretized state-space $\mathcal{X}_d$
b) ***Motion primitive generation:*** Compute the set of motion primitives $\mathcal{P}$ by specifying a set of desired maneuvers and solve (20) using an OCP solver
c) ***Heuristic function:*** Precompute a heuristic look-up table (HLUT) by computing the optimal cost-to-go on a grid in an obstacle-free environment

Step 1 – Online planning:
a) ***Initialization:*** Project the vehicle's initial state $\boldsymbol{x}_I$ and desired goal state $\boldsymbol{x}_G$ to $\mathcal{X}_d$
b) ***Graph search:*** Solve the discrete graph search problem (19) using a graph search algorithm

Step 2 – Homotopy-based optimization step:
a) ***Initialization:*** Initialize the homotopy-based OCP solver with the solution computed by the lattice planner
b) ***Optimization:*** Solve the relaxed trajectory planning problem (24) using an OCP solver
c) ***Return:*** Send the computed solution to a trajectory-tracking controller or report failure

where $l(\boldsymbol{x}^i, \boldsymbol{u}^i)$ is defined in (17). The resulting trajectory taken by the vehicle when motion primitive $\boldsymbol{m}_i \in \mathcal{P}$ is applied from $\boldsymbol{x}[k]$, is collision-free if it does not collide with any obstacle $c(\boldsymbol{m}_i, \boldsymbol{x}[k]) \in \mathcal{X}_{\text{free}}$. Define $u_p : \mathbb{Z}_+ \to \{1, \dots, M\}$ as a discrete and integer-valued decision variable that is selected by the lattice planner, where $u_p[k]$ specifies which motion primitive that is applied at stage k. Now, the continuous-time trajectory planning problem (16) is approximated by the following discrete-time OCP (Ljungqvist et al., 2019):

$$\begin{aligned} \underset{\{u_p[k]\}_{k=0}^{N_p-1},\, N_p}{\text{minimize}} \quad & J_D = \sum_{k=0}^{N_p-1} J_p(\boldsymbol{m}_{u_p[k]}) \\ \text{subject to} \quad & \boldsymbol{x}[k+1] = f_p(\boldsymbol{x}[k], \boldsymbol{m}_{u_p[k]}), \\ & \boldsymbol{x}[0] = \bar{\boldsymbol{x}}_I, \quad \boldsymbol{x}[N_p] = \bar{\boldsymbol{x}}_G, \\ & \boldsymbol{m}_{u_p[k]} \in \mathcal{P}(\boldsymbol{x}[k]), \\ & c(\boldsymbol{m}_{u_p[k]}, \boldsymbol{x}[k]) \in \mathcal{X}_{\text{free}}, \end{aligned} \tag{19}$$

for $k = 0, \dots, N_p - 1$, where $\bar{\boldsymbol{x}}_I$ and $\bar{\boldsymbol{x}}_G$ are obtained by projecting the actual initial state $\boldsymbol{x}_I$ and desired goal state $\boldsymbol{x}_G$ to the their closest neighboring state in $\mathcal{X}_d$. The decision variables to the problem in (19) are the motion primitive sequence $\{u_p[k]\}_{k=0}^{N_p-1}$ and its length $N_p \in \mathbb{Z}_+$. A feasible solution is an ordered sequence of collision-free motion primitives $\{\boldsymbol{m}_{u_p[k]}\}_{k=0}^{N_p-1}$, i.e., a trajectory $(\boldsymbol{x}(t), \boldsymbol{u}(t))$, $t \in [0, t_G]$ that connects the projected initial state $\boldsymbol{x}(0) = \bar{\boldsymbol{x}}_I$ with the projected goal state $\boldsymbol{x}(t_G) = \bar{\boldsymbol{x}}_G$. Given the set of all feasible solutions to (19), an optimal solution is one that minimizes the cost function J_{D}. During online planning, the discrete-time OCP in (19) can be solved using classical graph-search algorithms such as A* together with an informative precomputed free-space heuristic look-up table (HLUT) as heuristic function (Knepper and Kelly, 2006). A HLUT significantly reduces the online planning time, as it takes the vehicle's nonholonomic constraints into account and enables perfect estimation of cost-to-go in free-space scenarios with no obstacles.

3.1 State-space discretization

It is important that the resolution of the discretized state space $\mathcal{X}_d$ and the cardinality of the motion primitive set $\mathcal{P}$ are chosen such that the vehicle is sufficiently agile to maneuver in confined environments. However, as they also define the size of the lattice graph $\mathcal{G}$, both the resolution of $\mathcal{X}_d$ and the cardinality of $\mathcal{P}$ have to be chosen carefully in order to maintain a reasonable search time during online planning (Pivtoraiko et al., 2009). Motivated by this, the position of the Nth trailer $(x_N[k], y_N[k])$ is discretized to a uniform grid with resolution r and its orientation is irregularly [1] discretized $\theta_N[k] \in \Theta$ into $|\Theta| = 16$ different orientations as proposed in (Pivtoraiko et al., 2009). Additionally, the longitudinal velocity of the tractor is discretized as $v_0[k] \in V = \{-\bar{v}, 0, \bar{v}\}$, where $\bar{v}$ is the tractor's maximal allowed speed. All remaining vehicle states are constrained to zero at each vertex in the graph, which implies that the MSNT vehicle is arranged in a straight configuration. This means that the joint angles $\beta_i[k]$, $i = 1, \dots, N$, the steering angles $\beta_0[k]$, $\boldsymbol{\gamma}_s[k]$, the steering angle rates $\omega_0[k]$, $\boldsymbol{\omega}_s[k]$ as well as the longitudinal acceleration of the tractor $a_0[k]$ are all constrained to zero at each $\boldsymbol{x}[k] \in \mathcal{X}_d$. As a consequence, $\dim(\mathcal{X}_d) = 4$, since only the pose $\boldsymbol{p}_N[k]$ and the velocity of the tractor $v_0[k]$ are allowed to vary between different vertices in the graph. The proposed discretization will impose restrictions, but is motivated to enable fast online planning. Moreover, since the output from the lattice planner will be used to warm start a second optimization step, the initial guess computed by the lattice planner will be improved such that the finally computed trajectory is a locally optimal solution to the original trajectory planning problem (16).

3.2 Motion primitive generation

The motion primitives $\mathcal{P}$ is computed offline by solving a finite set of OCPs from all initial states $\boldsymbol{x}_s^i \in \mathcal{X}_d$ with the position of the Nth trailer at the origin, to a set of final states $\boldsymbol{x}_f^i \in \mathcal{X}_d$ in an obstacle-free environment. This procedure can be performed manually as in Ljungqvist et al. (2019) or using exhaustive search together with pruning strategies as proposed in Pivtoraiko et al. (2009); Cirillo et al. (2014). In both cases, the motion primitive generation procedure will become time consuming or requires a designer with high system knowledge. Therefore, here we use the maneuver-based motion primitive generation framework introduced in Bergman et al. (2019). Instead of selecting pairs of discrete vehicle states to connect, a set of desired maneuvers from each initial state $\boldsymbol{x}_s^i \in \mathcal{X}_d$ is selected and an OCP solver together with a rounding heuristic are used to automatically select the optimal final state $\boldsymbol{x}_f^i \in \mathcal{X}_d$. Each maneuver is defined with a terminal manifold in the form $\boldsymbol{g}^i(\boldsymbol{x}^i(t_f^i)) = 0$ where $\boldsymbol{g} : \mathbb{R}^n \to \mathbb{R}^l$ and $l < n$, where $n - l$ is the degrees of freedom for the terminal state constraint. To compute a maneuver-specified motion primitive $\boldsymbol{m}_i \in \mathcal{P}$, the following continuous-time OCP is first solved

$$\begin{aligned} \underset{\boldsymbol{u}^i(\cdot),\, t_p^i}{\text{minimize}} \quad & J_p(\boldsymbol{m}_i) \\ \text{subject to} \quad & \dot{\boldsymbol{x}}^i(t) = \boldsymbol{f}(\boldsymbol{x}^i(t), \boldsymbol{u}^i(t)), \\ & \boldsymbol{x}^i(0) = \boldsymbol{x}_s^i, \quad \boldsymbol{g}^i(\boldsymbol{x}^i(t_f^i)) = 0, \\ & \boldsymbol{x}^i(t) \in \mathcal{X}^i, \quad \boldsymbol{u}^i(t) \in \mathcal{U}^i. \end{aligned} \tag{20}$$

[1] Θ is the the set of unique angles $-\pi < \theta_N \leq \pi$ that can be generated by $\theta_N = \arctan 2(i, j)$ for two integers $i, j \in \{-2, -1, 0, 1, 2\}$.

Here it is not required that $\boldsymbol{x}^i(t_f^i) \in \mathcal{X}_d$. To ensure that the final state $\boldsymbol{x}_f^i = \boldsymbol{x}^i(t_f^i) \in \mathcal{X}_d$, a rounding heuristic is used and the closest neighboring states represented in the discretized state-space $\mathcal{X}_d$ from $\boldsymbol{x}^i(t_f^i)$ are evaluated and the solution with lowest objective functional value is selected as the resulting motion primitive $\boldsymbol{m}_i$. Finally, since the MSNT with a car-like tractor is orientation invariant, rotational symmetries are exploited to reduce the number of OCPs needed to be solved (Pivtoraiko et al., 2009). For more details of the motion primitive generation framework, the reader is referred to Bergman et al. (2019). Note that the vehicle's physical constraints $\mathcal{X}^i \subseteq \mathcal{X}$ and $\mathcal{U}^i \subseteq \mathcal{U}$ in (20) are defined to be maneuver dependent, which is not the case in Bergman et al. (2019). This extension is made to automatically generate similar maneuvers, i.e., same terminal manifold $\boldsymbol{g}^i(\boldsymbol{x}^i(t_f^i)) = 0$, but resulting in different optimal final states $\boldsymbol{x}_f^i$ and final times t_f^i. This additional freedom can be used to design a more flexible lattice planner or, e.g., to adapt to a change in available trailer steering angles γ_s, $s \in \mathcal{I}_s$ during different maneuvers.

As proposed in Bergman et al. (2019), the motion primitive set is built upon optimized straight, heading change and parallel maneuvers. The heading change and parallel maneuvers are only possible to use from states where the tractor has nonzero velocity, i.e. $v_{0,s} = \pm\bar{v}$, and are designed to end up in the same final velocity $v_{0,f} = v_{0,s}$. Additionally, short straight maneuvers from $v_{0,s} \in V$ to some $v_{0,f} \in V$ are also optimized to enable the tractor to reduce, increase and keep a constant longitudinal velocity.

Heading change maneuvers: By specifying the vehicle's physical constraints $\mathcal{X}^i \subseteq \mathcal{X}$ and $\mathcal{U}^i \subseteq \mathcal{U}$, a heading change maneuver from an initial state $\boldsymbol{x}_s^i \in \mathcal{X}_d$ with pose $\boldsymbol{p}_{N,s}^i = \begin{bmatrix} 0 & 0 & \theta_{N,s}^i \end{bmatrix}^\intercal$ and $v_{0,s}^i = \pm\bar{v}$, to a user-defined adjacent orientation $\theta_{N,f}^i \in \Theta \setminus \theta_{N,s}^i$ is optimized by solving (20) using the following terminal constraint

$$\boldsymbol{g}^i\left(\boldsymbol{p}_N^i(t_f^i), v_{0,f}^i\right) = \begin{bmatrix} \theta_N^i(t_f^i) - \theta_{N,f}^i \\ v_0^i(t_f^i) - v_{0,s}^i \end{bmatrix} = 0, \qquad (21)$$

which implies that $x_N^i(t_f)$ and $y_N^i(t_f)$ are free variables for the OCP solver to select. Note that the vehicle states that are left out from the argument to $\boldsymbol{g}^i$ are all constrained to zero to guarantee that $\boldsymbol{x}_f^i \in \mathcal{X}_d$. Examples of computed heading change maneuvers from $(\theta_{3,s}, v_{0,s}) = (\pi/2, \pm 1)$ are depicted in Fig. 2 for an MS3T vehicle with a car-like tractor where the last trailer has steerable wheels, i.e., $\mathcal{I}_s = \{3\}$. Here, the allowed trailer steering angle $|\gamma_3| \leq \bar{\gamma}_3$ is alternated using $\bar{\gamma}_3 = 0$, 0.175 and 0.35 rad, resulting in different types of optimal trajectories.

Parallel maneuvers: A parallel maneuver from an initial state $\boldsymbol{x}_s^i \in \mathcal{X}_d$ with pose $\boldsymbol{p}_{N,s}^i = \begin{bmatrix} 0 & 0 & \theta_{N,s}^i \end{bmatrix}^\intercal$ and $v_{0,s}^i = \pm\bar{v}$, is defined with a user-defined lateral displacement z_{lat}^i in $(x_{N,f}^i, y_{N,f}^i)$ with respect to the initial orientation $\theta_{N,s}^i$. This maneuver can be optimized by solving (20) using a terminal constraint $\boldsymbol{g}^i(\boldsymbol{p}_N^i(t_f), v_{0,f}^i) = 0$, where

$$\boldsymbol{g}^i\left(\boldsymbol{p}_N^i(t_f^i), v_{0,f}^i\right) = \begin{bmatrix} y_N^i(t_f^i)\cos\theta_{N,s}^i + x_N^i(t_f^i)\sin\theta_{N,s}^i - z_{\text{lat}}^i \\ \theta_N^i(t_f^i) - \theta_{N,s}^i \\ v_0^i(t_f^i) - v_{0,s}^i \end{bmatrix} \qquad (22)$$

Here, the final position of the Nth trailer $(x_N(t_f^i), y_N(t_f^i))$ is restricted to a line defined by the first row in (22).

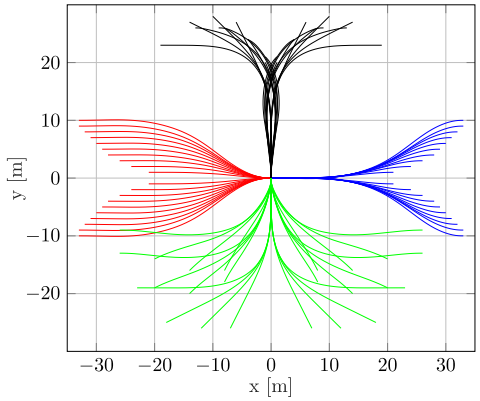

Fig. 2. A subset of the motion primitives in $\mathcal{P}$ for an MS3T vehicle with a car-like tractor from initial position at the origin $(x_{3,s}, y_{3,s}) = (0, 0)$ to different final states $\boldsymbol{x}_f \in \mathcal{X}_d$. The colored lines are the trajectories in $(x_3(\cdot), y_3(\cdot))$ for the different maneuvers. The set of heading change maneuvers from $(\theta_{3,s}, v_{0,s}) = (\pi/2, 1)$ (black) and from $(\theta_{3,s}, v_{0,s}) = (\pi/2, -1)$ (green). The set of parallel maneuvers from $(\theta_{3,s}, v_{0,s}) = (0, 1)$ (blue) and from $(\theta_{3,s}, v_{0,s}) = (0, -1)$ (red).

Examples of computed parallel maneuvers for an MS3T vehicle with a car-like tractor using $\bar{\gamma}_3 = 0.35$ rad from $(\theta_{3,s}, v_{0,s}) = (0, \pm 1)$ can be seen in Fig. 2.

When the motion primitive set $\mathcal{P}$ is computed, a free-space heuristic look-up table (HLUT) is computed using techniques presented in Knepper and Kelly (2006). The HLUT is computed offline by solving several obstacle-free graph-search problems (19) from all initial states $\bar{\boldsymbol{x}}_I \in \mathcal{X}_d$ with $(x_{N,I}, y_{N,I}) = (0, 0)$, to final states $\bar{\boldsymbol{x}}_G \in \mathcal{X}_d$ with positions on a bounded grid around the origin. This computation can be done efficiently using Dijkstra's search, as the optimal cost-to-come is simply recorded and stored in the HLUT (Knepper and Kelly, 2006).

4. HOMOTOPY-BASED OPTIMIZATION STEP

Similar to (Bergman et al., 2020), the optimization step is used to improve the initial guess $(\boldsymbol{x}(t), \boldsymbol{u}(t))$, $t \in [0, t_G]$ computed by the lattice planner such that the final trajectory $(\boldsymbol{x}^*(t), \boldsymbol{u}^*(t))$, $t \in [0, t_G^*]$ is a locally optimal solution to (16). Since the lattice planner uses a discretized state space $\mathcal{X}_d$, in general its computed state trajectory does not satisfy the initial and goal state constraints in (19). Thus, the optimization step should not only improve the initial guess but also make it feasible in the original problem formulation (16). To handle this in a structured way, a homotopy-based initialization strategy is used that is inspired by the work in Bergman and Axehill (2018). The idea is to start from a relaxed problem that is easy to solve and then gradually transform the relaxed problem to the original one. Here, these ideas are applied on the initial and goal state constraints in (16) such that the solution obtained from the lattice planner is feasible to the relaxed problem. By letting $\boldsymbol{\epsilon}_p^\intercal = [\epsilon_{p,I} \;\; \epsilon_{p,G}] \in [0, 1]^2$ denote the homotopy parameters (Bergman and Axehill, 2018), the initial and goal state constraints in (16) are relaxed to

$$\begin{aligned} \boldsymbol{x}(0) &= \epsilon_{p,I}\bar{\boldsymbol{x}}_I + (1 - \epsilon_{p,I})\boldsymbol{x}_I, \\ \boldsymbol{x}(t_G) &= \epsilon_{p,G}\bar{\boldsymbol{x}}_G + (1 - \epsilon_{p,G})\boldsymbol{x}_G. \end{aligned} \qquad (23)$$

When $\boldsymbol{\epsilon}_p^\intercal = [1 \;\; 1]$, the initial guess from the lattice planner is feasible in the relaxed version of (16) and when $\boldsymbol{\epsilon}_p^\intercal = [0 \;\; 0]$, the original problem in (16) is obtained. One possibility is to start with $\boldsymbol{\epsilon}_p^0 = [1 \;\; 1]^\intercal$ and repeatedly solve the relaxed version of (16) using an OCP solver

where $\boldsymbol{\epsilon}_p^k$ is gradually decreased using a fixed step-size $\Delta\boldsymbol{\epsilon}_p$ until $\boldsymbol{\epsilon}_p^k = [0\ 0]^\mathsf{T}$ is reached (Bergman and Axehill, 2018). In this work, the idea is instead to let the OCP solver automatically modify the homotopy parameters using a penalty method (Nocedal and Wright, 2006). Define the linear penalty as $\boldsymbol{c}_p^\mathsf{T}\boldsymbol{\epsilon}_p$, where $\boldsymbol{c}_p \in \mathbb{R}^2_{++}$ and define the relaxed version of the trajectory planning problem (16) as

$$\begin{aligned} \underset{\boldsymbol{u}(\cdot),\, t_G,\, \boldsymbol{\epsilon}_p}{\text{minimize}} \quad & J_H = J + \boldsymbol{c}_p^\mathsf{T}\boldsymbol{\epsilon}_p \\ \text{subject to} \quad & \dot{\boldsymbol{x}}(t) = \boldsymbol{f}(\boldsymbol{x}(t), \boldsymbol{u}(t)), \\ & \boldsymbol{x}(0) = \epsilon_{p,I}\bar{\boldsymbol{x}}_I + (1-\epsilon_{p,I})\boldsymbol{x}_I, \\ & \boldsymbol{x}(t_G) = \epsilon_{p,G}\bar{\boldsymbol{x}}_G + (1-\epsilon_{p,G})\boldsymbol{x}_G, \\ & \boldsymbol{x}(t) \in \mathcal{X}_{\text{free}}, \quad \boldsymbol{u}(t) \in \mathcal{U}, \quad \boldsymbol{\epsilon}_p \in [0,1]^2, \end{aligned} \tag{24}$$

which is initialized with the solution from the lattice planner and $\boldsymbol{\epsilon}_p^\mathsf{T} = [1\ 1]$. By choosing $\boldsymbol{c}_p$ sufficiently large, the OCP solver will automatically adjust the step size of $\boldsymbol{\epsilon}_p$ and converge to $\boldsymbol{\epsilon}_p^\mathsf{T} = [0\ 0]$ if a feasible solution to (16) exists in the homotopy class selected by the lattice planner (19) (Bergman and Axehill, 2018). As previously mentioned, if $\boldsymbol{\epsilon}_p^* = [0\ 0]^\mathsf{T}$ is obtained, a locally optimal solution $(\boldsymbol{x}^*(t), \boldsymbol{u}^*(t))$, $t \in [0, t_G^*]$ to the original trajectory planning problem (16) is obtained which can then be sent to a trajectory-tracking controller for plan execution.

Note that if $\boldsymbol{c}_p$ is not chosen sufficiently large, a solution with $\boldsymbol{\epsilon}_p^\mathsf{T} = [0\ 0]$ may not be obtained even though one exists (Nocedal and Wright, 2006). In that case, one may need to increase $\boldsymbol{c}_p$ and continue the solution process. However, in extensive simulation trials presented in Section 5, it is shown that the proposed homotopy-based optimization step is able to reliably compute locally optimal solutions to (24) with $\boldsymbol{\epsilon}_p^\mathsf{T} = [0\ 0]$ without modifying $\boldsymbol{c}_p$ in all problem instances.

5. SIMULATION RESULTS

In this section, the proposed trajectory planning framework is evaluated in two complicated parking problem scenarios for an MS3T with a car-like tractor where only trailer $N = 3$ is steerable, i.e., $\mathcal{I}_s = \{3\}$, and a mixture of off-axle ($M_1 \neq 0$) and on-axle hitching ($M_2 = M_3 = 0$) is used. Using the recursive model presented in Section 2 it is now straightforward to derive the kinematic vehicle model (15) with configuration $\boldsymbol{q}^\mathsf{T} = [\beta_0\ \beta_1\ \beta_2\ \beta_3\ \gamma_3\ \theta_3\ x_3\ y_3]$, augmented state vector $\boldsymbol{x}^\mathsf{T} = [\boldsymbol{q}^\mathsf{T}\ \omega_0\ \omega_3\ v_0\ a_0]$ and control signals $\boldsymbol{u}^\mathsf{T} = [u_{\omega_0}\ u_{\omega_3}\ u_v]$. Thus, $\dim(\boldsymbol{x}) = 12$ and $\dim(\boldsymbol{u}) = 3$. The values of the vehicle's parameters used in this section are summarized in Table 1. The cost function is chosen as

$$l(\boldsymbol{x}, \boldsymbol{u}) = \frac{1}{2}\left(\beta_0^2 + \gamma_s^2 + 10\omega_0^2 + 10\omega_3^2 + a_0^2 + \boldsymbol{u}^\mathsf{T}\boldsymbol{u}\right), \tag{25}$$

which is used in all steps of the trajectory planning framework. The linear cost on the homotopy parameters in the optimization step is chosen as $c_p^\mathsf{T} = [1000\ 1000]$. The obstacles and vehicle bodies are described by bounding circles (LaValle, 2006), where in total, the vehicle bodies are described using 8 bounding circles of radius 2 m. The lattice planner is implemented in `C++`, whereas the motion primitive generation and the homotopy-based optimization step are both implemented in Python using CasADi (Andersson et al., 2018), where IPOPT is used as nonlinear programming problem solver. All simulations are performed on a standard laptop computer with an Intel Core i7-4600U@2.1GHz CPU.

Table 1. Vehicle parameters for the MS3T vehicle.

Vehicle parameter	Value
Tractor's wheelbase L_0	4.6 m
Length of the off-hitch M_1	1.6 m
Length of trailer 1 L_1	2.5 m
Length of trailer 2 L_2	7.0 m
Length of trailer 3 L_3	7.0 m
Maximum joint angles $\bar{\beta}_i$, $i = 1, 2, 3$	0.87 rad
Maximum steering angle tractor $\bar{\beta}_0$	0.73 rad
Maximum steering-angle rate tractor $\bar{\omega}_0$	0.8 rad/s
Maximum steering-angle acceleration tractor $\bar{\Omega}_0$	10 rad/s^2
Maximum steering angle trailer 3 $\bar{\gamma}_3$	0.35 rad
Maximum steering-angle rate trailer 3 $\bar{\omega}_3$	0.4 rad/s
Maximum steering-angle acceleration trailer 3 $\bar{\Omega}_3$	10 rad/s^2
Maximum longitudinal speed tractor $\bar{v}$	1 m/s
Maximum longitudinal acceleration tractor $\bar{a}$	1 m/s^2
Maximum longitudinal jerk tractor $\bar{u}_v$	40 m/s^2

The motion primitive set consists of heading change, parallel and straight maneuvers where a subset of the motion primitive set $\mathcal{P}_{\text{MS3T}}$ ($|\mathcal{P}_{\text{MS3T}}| = 2080$) can be seen in Fig. 2. From each initial heading with nonzero longitudinal velocity, there are 20 parallel and 24 heading change maneuvers. The heading change maneuvers are computed using three different limits on the trailer steering angle $\bar{\gamma}_3 = 0$, 0.175 and 0.35 rad, respectively, and the parallel maneuvers using $\bar{\gamma}_3 = 0.35$ rad. After the motion primitive set is computed, a free-space HLUT is computed on a square grid 80×80 m centered around the origin. To evaluate if the trajectory planner is able to exploit the additional trailer steering, it is compared with an SS3T vehicle, i.e., $\bar{\gamma}_3 = 0$, with the same vehicle parameters and the difference that only 8 heading change maneuvers exist in the motion primitive set $\mathcal{P}_{\text{SS3T}}$ ($|\mathcal{P}_{\text{SS3T}}| = 1124$).

The first planning scenario is a loading-bay parking problem that is illustrated in Fig. 3. The objective of the trajectory planner is to plan a trajectory from 32 different initial states $\boldsymbol{x}_I \in \mathcal{X}_d$ (see Fig. 3) to the goal state $\boldsymbol{x}_G$. One solution example is provided for the lattice planner (dashed line) and optimization step (solid line) for SS3T (orange) and MS3T (green), respectively, for symmetric planning problems. The results show that the planned trajectory for MS3T is purely in backward motion, compared to SS3T which needs to combine forward and backward motion due to less steering capability. A summary of the simulation results are provided in Table 2. The average computation time for the lattice planner is only 0.1 s for both SS3T and MS3T, whereas the optimization step takes in average 3.0 s for MS3T and 9.0 s for SS3T. However, a signification reduction of both average cost and time improvement of the solutions are obtained. Note that the average time improvement of the solutions computed by the optimization step $\bar{t}_{G,\text{imp}}$ is significantly larger than the optimization step's average computation time $\bar{t}_{\text{ocp}}$. Thus, when the optimization step is added, the sum of the average computation and execution time becomes lower.

Table 2. Results from loading-bay parking scenario in Fig. 3 for 32 problems. $\bar{t}_{\text{lat}}$ and $\bar{t}_{\text{ocp}}$ is average computation time for lattice planner and optimization step, respectively. $\bar{J}_D$ and $\bar{J}_H$ is average objective functional value for the solutions from lattice planner and optimization step, respectively. $\bar{r}_{\text{imp}}$ and $\bar{t}_{G,\text{imp}}$ is average cost and time improvement between the lattice planner's and the optimization step's solutions, respectively.

Vehicle	$\bar{t}_{\text{lat}}$[s]	$\bar{t}_{\text{ocp}}$[s]	$\bar{J}_D$	$\bar{J}_H$	$\bar{r}_{\text{imp}}$	$\bar{t}_{G,\text{imp}}$[s]
SS3T	0.11	9.3	170.8	128.4	-25%	-26.8
MS3T	0.09	3.0	126.8	100.8	-21%	-14.4

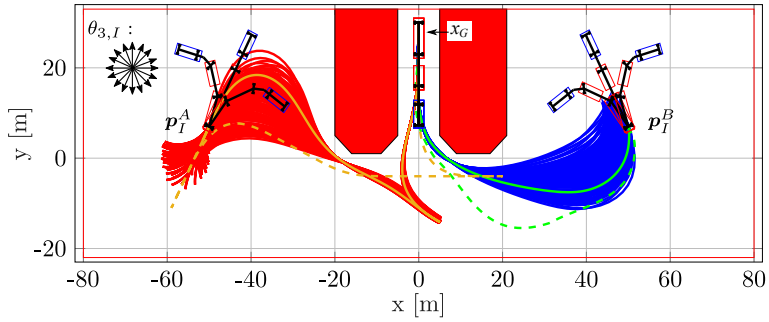

Fig. 3. Loading-bay parking scenario using the proposed trajectory planner for SS3T and MS3T from two initial positions ($\boldsymbol{p}_I^A$ and $\boldsymbol{p}_I^B$), symmetric with respect to the loading bay, initial orientations $\theta_{3,I} \in \Theta$ and zero initial joint angles, to the goal state $\boldsymbol{x}_G$. The solutions for the position $(x_3^*(\cdot), y_3^*(\cdot))$ from 1029 perturbed initial states for SS3T ($\boldsymbol{p}_I^A$) and MS3T ($\boldsymbol{p}_I^B$) are displayed by blue (red) solid lines for MS3T (SS3T). The initial guess computed by the lattice planner for $(x_3(\cdot), y_3(\cdot))$ and optimization step for $(x_3^*(\cdot), y_3^*(\cdot))$ from straight configuration is marked with green (orange) dashed line and green (orange) solid line, respectively, for MS3T (SS3T).

To evaluate how the homotopy-based optimization step handles an infeasible initialization, 1029 perturbed initial states for both SS3T and MS3T are evaluated (see Fig. 3), where blue and red trajectories are related to MS3T and SS3T, respectively. The initial joint angles are perturbed with $\beta_i = -30°, -20°, \ldots, 30°$, $i = 1, 2, 3$ and initial orientation with $\theta_{3,I} = -10°, 0°, 10°$. In all cases, the used optimization step is able to handle the infeasible initial guess obtained from the lattice planner, i.e., the value of the computed optimal homotopy parameter is $\epsilon_{p,I}^* = 0$ in all cases. That is, in all cases, a solution to the original trajectory planning problem (16) is obtained. Moreover, the average computation time of the optimization step is 3.4 s for MS3T and 26.2 s for SS3T. Hence, the active trailer steering seems to reduce the computation time of the OCP solver.

The second planning scenario is a parallel parking problem with 18 different problem instances that is illustrated in Fig. 5 and the results are summarized in Table 3. This scenario is a confined environment which affects the average computation time of the lattice planner $\bar{t}_{\text{lat}}$, which is 11.3 s for MS3T and 5.6 s for SS3T. This is because the HLUT is drastically underestimating the cost-to-go in this confined environment. Because of the confined environment, both the average cost improvement $\bar{r}_{\text{imp}}$ (MS3T: -52%, SS3T: -55%) and time improvement $\bar{t}_{G,\text{imp}}$ (MS3T: -80.4 s, SS3T: -109.6 s) of the optimization step are significant. The confined environment does however not significantly affect the average computation time of the optimization step which is 2.4 s for MS3T and 8.4 s for SS3T. Moreover, as can be seen in the three highlighted planning problems in Fig. 5, the final optimized solutions for the MS3T only need to reverse, as opposed to the SS3T which needs to combine forward and backward motion in two cases. Finally, Fig. 4 shows the difference between the trajectories from the lattice planner and the optimization step for the selected planning problem from position $\boldsymbol{p}_I^3$ in Fig. 5. As can be seen, the state trajectories for the two steering angles, the longitudinal velocity and the joint angles are significantly smoother after the optimization step, at the same time as the final time is decreased from 96 s to 70 s.

6. CONCLUSION

An optimization-based trajectory planner for multi-steered articulated vehicles is proposed that targets low-speed maneuvers in unstructured environments. The proposed trajectory planner is divided into two steps, where a lattice planner is used in a first step to compute an optimal solution to a discretized version of the trajectory planning problem using a library of precomputed trajectories. In a second step, the output from the lattice planner is then used to initialize a homotopy-based optimization step, which enables the framework to compute a locally optimal solution that starts at the vehicle's initial state and reaches the goal state exactly. The performance of the proposed optimization-based trajectory planner is evaluated in a set of practically relevant scenarios for a multi-steered 3-trailer vehicle where the last trailer is steerable. In the simulations, it is shown that the framework can solve challenging trajectory planning problems and that the proposed optimization step provides a significant improvement in terms of reduced objective functional value and final time, at the same time as it enables the framework to plan from and to a larger set of different vehicle states.

As future work we would like to develop a trajectory-tracking controller and evaluate the framework in real-world experiments on a full-scale test vehicle.

Table 3. Results from parallel parking scenario in Fig. 5 for 18 problems. See Table 2 for description of the variables.

Vehicle	$\bar{t}_{\text{lat}}$[s]	$\bar{t}_{\text{ocp}}$[s]	$\bar{J}_D$	$\bar{J}_H$	$\bar{r}_{\text{imp}}$	$\bar{t}_{G,\text{imp}}$[s]
SS3T	5.6	8.4	270.6	122.4	-55%	-109.6
MS3T	11.3	2.4	207.9	98.1	-52%	-80.4

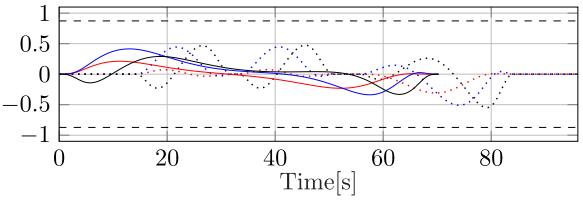

(a) The joint angle between tractor and trailer 1 $\beta_1(\cdot)$ (black), joint angle between the trailer 1 and trailer 2 $\beta_2(\cdot)$ (blue), and joint angle between the trailer 2 and trailer 3 $\beta_3(\cdot)$ (red). Their limits are displayed by dashed black lines.

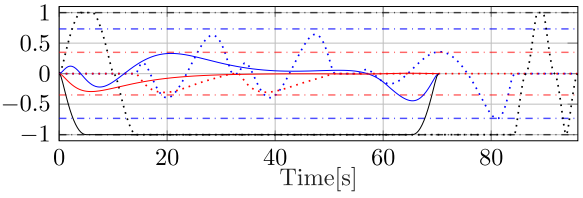

(b) The steering angle of the tractor β_0 (blue), velocity v_0 (black) and steering angle of trailer 3 γ_3 (red). Their limits are displayed by dashed-dotted lines.

Fig. 4. A subset of the resulting state trajectories for the parallel parking scenario in Fig. 5 from initial state $\boldsymbol{p}_I^3$ with MS3T for optimized (solid lines) and lattice initial guess (dotted lines).

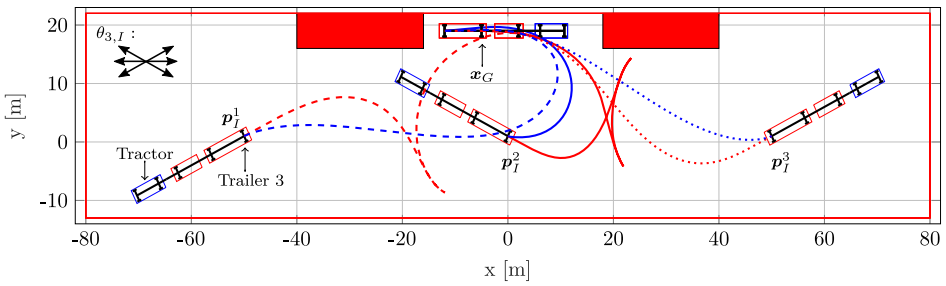

Fig. 5. Parallel parking scenario using the proposed trajectory planner for SS3T and MS3T from three different initial positions ($\boldsymbol{p}_I^1$, $\boldsymbol{p}_I^2$ and $\boldsymbol{p}_I^3$), six different initial orientations $\theta_{3,I}$ and zero initial joint angles, to the goal state $\boldsymbol{x}_G$. The blue (red) lines illustrate the planned trajectories after the optimization step for the position of trailer 3 ($x_3^*(\cdot), y_3^*(\cdot)$) for MS3T (SS3T) from three selected initial states.

REFERENCES

Andersson, J.A.E. et al. (2018). CasADi – A software framework for nonlinear optimization and optimal control. *Mathematical Programming Computation*.

Bergman, K. and Axehill, D. (2018). Combining homotopy methods and numerical optimal control to solve motion planning problems. In *Proceedings of the 2018 IEEE Intelligent Vehicles Symposium*, 347–354.

Bergman, K., Ljungqvist, O., and Axehill, D. (2019). Improved optimization of motion primitives for motion planning in state lattices. In *Proceedings of the 2019 IEEE Intelligent Vehicles Symposium*.

Bergman, K., Ljungqvist, O., and Axehill, D. (2020). Improved path planning by tightly combining lattice-based path planning and optimal control. *Accepted for publication in IEEE Transactions on Intelligent Vehicles*. Pre-print available at arXiv: `https://arxiv.org/abs/1903.07900`.

Beyersdorfer, S. and Wagner, S. (2013). Novel model based path planning for multi-axle steered heavy load vehicles. In *Proceedings of the 16th International Conference on Intelligent Transportation Systems*, 424–429.

Bushnell, L.G. et al. (1995). Steering three-input nonholonomic systems: the fire truck example. *The International Journal of Robotics Research*, 14(4), 366–381.

Cirillo, M., Uras, T., and Koenig, S. (2014). A lattice-based approach to multi-robot motion planning for non-holonomic vehicles. In *Proceedings of the 2014 IEEE/RSJ International Conference on Intelligent Robots and Systems*, 232–239.

Evestedt, N., Ljungqvist, O., and Axehill, D. (2016). Motion planning for a reversing general 2-trailer configuration using Closed-Loop RRT. In *Proceedings of the 2016 IEEE/RSJ International Conference on Intelligent Robots and Systems*, 3690–3697.

Islam, M.M. et al. (2015). A comparative study of multi-trailer articulated heavy-vehicle models. *Proceedings of the Institution of Mechanical Engineers, Part D: Journal of Automobile Engineering*, 229(9), 1200–1228.

Knepper, R.A. and Kelly, A. (2006). High performance state lattice planning using heuristic look-up tables. In *Proceedings of the 2006 IEEE/RSJ International conference on Intelligent Robots and Systems*, 3375–3380.

Lamiraux, F. et al. (1999). Motion planning and control for hilare pulling a trailer. *IEEE Transactions on Robotics and Automation*, 15(4), 640–652.

LaValle, S.M. (2006). *Planning algorithms*. Cambridge University Press.

Li, B. et al. (2019). Tractor-trailer vehicle trajectory planning in narrow environments with a progressively constrained optimal control approach. *IEEE Transactions on Intelligent Vehicles*.

Ljungqvist, O. et al. (2019). A path planning and path-following control framework for a general 2-trailer with a car-like tractor. *Journal of Field Robotics*, 36(8), 1345–1377.

Michalek, M.M. (2019). Modular approach to compact low-speed kinematic modelling of multi-articulated urban buses for motion algorithmization purposes. In *Proceeding of the 2019 IEEE Intelligent Vehicles Symposium*, 2060–2065.

Nocedal, J. and Wright, S. (2006). *Numerical optimization*. Springer Science & Business Media.

Odhams, A. et al. (2011). Active steering of a tractor–semi-trailer. *Proceedings of the Institution of Mechanical Engineers, Part D: Journal of Automobile Engineering*, 225(7), 847–869.

Orosco-Guerrero, R. et al. (2002). Modeling and dynamic feedback linearization of a multi-steered n-trailer. *IFAC Proceedings Volumes*, 35(1), 103–108.

Pivtoraiko, M. et al. (2009). Differentially constrained mobile robot motion planning in state lattices. *Journal of Field Robotics*, 26(3), 308–333.

Sekhavat, S. et al. (1998). Multilevel path planning for nonholonomic robots using semiholonomic subsystems. *The International Journal of Robotics Research*, 17(8), 840–857.

Tilbury, D. et al. (1995). A multisteering trailer system: conversion into chained form using dynamic feedback. *IEEE Transactions on robotics and automation*, 11(6), 807–818.

Van De Wouw, N. et al. (2015). Active trailer steering for robotic tractor-trailer combinations. In *Proceeding of the 54th IEEE Conference on Decision and Control*, 4073–4079.

Varga, B. et al. (2018). Robust tracking controller design for active dolly steering. *Proceedings of the Institution of Mechanical Engineers, Part D: Journal of Automobile Engineering*, 232(5), 695–706.

Vidal-Calleja, T., Velasco-Villa, M., and Aranda-Bricaire, E. (2002). Real-time obstacle avoidance for trailer-like systems. In *Proceeding of the 3th International Symposium on Robotics and Automation*.

Wächter, A. and Biegler, L.T. (2006). On the implementation of a primal-dual interior point filter line search algorithm for large-scale nonlinear programming. *Mathematical Programming*, 106(1), 25–57.

Yuan, J. (2017). Hierarchical motion planning for multi-steering tractor-trailer mobile robots with on-axle hitching. *IEEE/ASME Transactions on Mechatronics*, 22(4), 1652–1662.

Zhang, X., Liniger, A., and Borrelli, F. (2020). Optimization-based collision avoidance. *IEEE Transactions on Control Systems Technology*, 1–12.